Dissipation Element Analysis of a Turbulent Non-Premixed Jet Flame

Michael Gauding[b),1,a)] Felix Dietzsch[b),2] Jens Henrik Goebbert,[3] Dominique Thévenin,[4] Abouelmagd Abdelsamie,[4] and Christian Hasse[2]

[1)] *CORIA CNRS UMR 6614, University of Rouen, France*

[2)] *Numerical Thermo-Fluid Dynamics, TU Bergakademie Freiberg, Germany*

[3)] *Juelich Supercomputing Center (JSC), Research Center Juelich, Germany*

[4)] *Lab. of Fluid Dynamics and Technical Flows, Otto von Guericke University of Magdeburg, Germany*

The objective of the present work is to examine the interaction between turbulent mixing and chemistry by employing the method of dissipation elements in a non-premixed turbulent jet flame. The method of dissipation elements (L. Wang and N. Peters, J. Fluid Mech., 554 (2006): 457-475) is used to perform a space-filling decomposition of the turbulent jet flow into different regimes conditioned on their location with respect to the reaction zone. Based on the non-local structure of dissipation elements this decomposition allows to discern whether points away from stoichiometry are connected through a diffusive layer with the reaction zone. In a next step, a regime based statistical analysis of dissipation elements is carried out by means of data obtained from a direct numerical simulation. Turbulent mixing and chemical reactions depend strongly on the mixture fraction gradient. From a budget between strain and dissipation the mechanism for the formation and destruction of mean gradients along dissipation elements is inspected. This budget reveals that large gradients in the mixture fraction field occur at a small but finite length scale. Finally, the inner structure of dissipation elements is examined by computing statistics along gradient trajectories of the mixture fraction field. Thereby, the method of dissipation elements provides a statistical characterization of flamelets and novel insight into the interaction between chemistry and turbulence.

PACS numbers: Valid PACS appear here

[a)] Electronic mail: michael.gauding@coria.fr ,[b)] Joint first authors

I. INTRODUCTION

The coupling between small-scale turbulent mixing and chemistry plays an important role for turbulent non-premixed flames. Under the assumption of fast chemistry, combustion in turbulent non-premixed flames takes place in thin layers around stoichiometric mixture. Away from stoichiometry the temperature declines and radicals recombine. In this region mainly turbulent mixing of stable species occurs. In a two-feed system the mixing state can be quantified by the mixture fraction,

$$Z = \frac{\dot{m}_{\text{fuel}}}{\dot{m}_{\text{fuel}} + \dot{m}_{\text{oxidizer}}}\,, \tag{1}$$

defined as the local ratio of the mass flux originating from the fuel feed $\dot{m}_{\text{f}}$ to the sum of the mass fluxes from both fuel and oxidizer feeds. The local mixing rate is characterized by the scalar dissipation rate

$$\chi = 2D\left(\frac{\partial Z}{\partial x_i}\right)^2\,, \tag{2}$$

which is proportional to the molecular diffusivity D and to the mixture fraction gradient squared. Here, summation over repeated indices is implied. Large local values of the scalar dissipation rate enhance turbulent mixing and increase the heat release, but may also result in extinction. Then radicals leak through the reaction zone and the temperature at stoichiometric mixture drops as diffusive heat loss exceeds heat release.

Flamelet models[1,2] have succeeded in predicting the combustion in non-premixed flames. They can be derived by an asymptotic analysis, where the turbulent flame is viewed as an ensemble of thin laminar flame structures. The flamelet theory is a multi-scale approach and introduces the mixture fraction Z as an independent coordinate. The scalar dissipation rate appears in the flamelet equations as a diffusion coefficient in mixture fraction space and accounts for the effect of turbulent mixing. Flamelets are non-local structures in the turbulent mixture fraction field, and consist of a mixing and an embedded reaction zone located around stoichiometric mixture. Flamelets are defined along gradient trajectories of the mixture fraction field[3], where the gradient trajectories are defined by the gradient direction

$$n_i = \frac{1}{\|\nabla Z\|}\frac{\partial Z}{\partial x_i}, \tag{3}$$

which points normal to the iso-surface of the mixture fraction field towards the fuel side. The solution of the flamelet equations is known as a function of mixture fraction Z and

can be mapped along gradient trajectories in the mixture fraction field. Therefore, gradient trajectories are important to examine mixing and combustion in turbulent non-premixed flames. The governing equation of the mixture fraction field $Z(\boldsymbol{x}, t)$ can be written in projected form along the direction of a gradient trajectory[4]

$$\rho\frac{\partial Z}{\partial t} + \rho u_n \frac{\partial Z}{\partial n} = \rho D \frac{\partial^2 Z}{\partial n^2} - \rho D \kappa_Z \frac{\partial Z}{\partial n} + \frac{\partial(\rho D)}{\partial n}\frac{\partial Z}{\partial n}\,, \tag{4}$$

where $u_n = u_i n_i$ denotes the velocity projected along the gradient trajectory,

$$\frac{\partial}{\partial n} = n_i \frac{\partial}{\partial x_i} \tag{5}$$

denotes the derivative in the direction of the mixture fraction gradient, and

$$\kappa_Z = -\frac{\partial n_i}{\partial x_i} \tag{6}$$

is the local curvature of the mixture fraction field, respectively. The last term of eq. (4) accounts for the effect of spatially varying density ρ and diffusivity D.

Diffusive transport occurs in turbulent fields predominantly along gradient trajectories which are aligned normally to the iso-surfaces of the mixture fraction field. Gradient trajectories, which constitute the flamelet coordinates, can be constructed by tracing the mixture fraction field in the direction of the ascending and descending gradient until a local maximum or minimum point is reached. The ending points represent critical points of the mixture fraction field, where the direction of the gradient trajectory is undefined, and the Hessian of Z is either positive definite (local minimum point) or negative definite (local maximum point). Within the gradient trajectory the mixture fraction varies monotonously. Gradient trajectories were first used by Peters and Trouillet[3] to study turbulent mixing in a core region of a shear layer and later by Wang and Peters[5,6] in homogeneous shear turbulence. Wang and Peters[5,6] defined the ensemble of gradient trajectories that share the same pair of maximum and minimum points as a dissipation element. Dissipation elements are irregular in shape and define coherent non-arbitrary regions. These regions are space-filling, which implies that all parts of the flow are covered when computing statistics over dissipation elements. Dissipation elements may be characterized by simple parameters derived from the information at the ending points. Wang and Peters[5,6] proposed to use the scalar difference

$$\Delta Z = Z_{\max} - Z_{\min} \tag{7}$$

and the linear distance ℓ between the ending points. These parameters describe the fluctuation intensity of the mixture fraction field at length scale ℓ. Wang and Peters[5,6] showed that the mean linear distance ℓ_m between the extremal points is of the order of the Taylor micro-scale λ. They argued that dissipation elements form coherent structures which are diffusively connected at length scales being much larger than the Kolmogorov scale η or Batchelor scales η_B. A schematic of a two-dimensional dissipation element is depicted in fig. 1. As a third independent parameter Peters and Trouillet[3] introduced additionally the arithmetic mean,

$$Z_{\mathrm{m}} = \frac{Z_{\max} + Z_{\min}}{2}\,, \tag{8}$$

of the mixture fraction between the ending points. The arithmetic mean Z_{m} describes in conjunction with ΔZ the precise location of the gradient trajectory in mixture fraction space. The three parameters ℓ, ΔZ, and Z_{m} contain from a statistical point of view most of the information about the mixture fraction field. A dissipation element based mean mixture fraction gradient g can be defined as

$$g = \frac{\Delta Z}{\ell}\,, \tag{9}$$

For brevity, we refer to g as mean gradient in the following. Due to the monotonicity of the mixture fraction along a gradient trajectory g has a positive, non-vanishing mean. Moreover, g is proportional to the mean diffusive flux between extremal points connected through gradient trajectories. The mean gradient g plays an important role to examine the efficiency of turbulent mixing because the second order moment of g can be related on dimensional grounds to the mean scalar dissipation

$$\langle g^2 \rangle \propto \frac{\langle \chi \rangle}{D}\,. \tag{10}$$

It is important to emphasis the difference between the scalar difference ΔZ of dissipation elements and the scalar increment $\delta_r Z = Z(\boldsymbol{x} + \boldsymbol{r}) - Z(\boldsymbol{x})$. The scalar increment $\delta_r Z$ is computed continuously along a straight line and the separation distance $\boldsymbol{r}$ between the two points is fixed in advance. While, on the other hand, for dissipation elements the scalar difference ΔZ is conditioned on local extremal points which are connected through gradient trajectories. The length scale ℓ results from the turbulent field itself, rather than being prescribed externally. This way of averaging is therefore able to capture information about the local structure of a turbulent field, which is otherwise averaged-out.

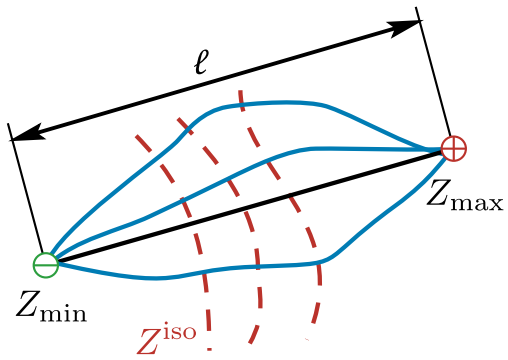

FIG. 1. Schematic of a two-dimensional dissipation element. Single gradient trajectories are illustrated by blue lines and connect a local minimum point ($Z_{\min}$) with a local maximum point ($Z_{\max}$) of the mixture fraction field. Gradient trajectories are oriented normal to the iso-lines of the mixture fraction field (red, dashed).

The objective of the present work is to analyze a direct numerical simulation of a turbulent non-premixed jet flame to examine the interaction between turbulence and chemistry by employing the method of dissipation elements. The method of dissipation elements is utilized as a post-processing technique to detect gradient trajectories. The paper is organized in the following way. We begin in sec. II with a brief overview of the direct numerical simulation (DNS) on which the analysis with dissipation elements is based. In sec. III we carry out a zonal decomposition of the non-premixed flame based on the ending points of dissipation elements and introduce three different regimes. This decomposition allows us to examine whether points away from stoichiometric mixture are linked through a diffusive layer with the surface of stoichiometric mixture. In sec. IV we present several statistical properties of dissipation elements and discuss cliff-ramp-like structures. From a balance between strain and diffusion we explain in sec. V the mechanism for the formation and destruction of mean gradients along dissipation elements. Finally, we examine in sec. VI the inner structure of dissipation elements and compute statistics along individual gradient trajectories to show how a mixture fraction gradient along gradient trajectories affects chemical reaction. Concluding remarks are given in sec. VII.

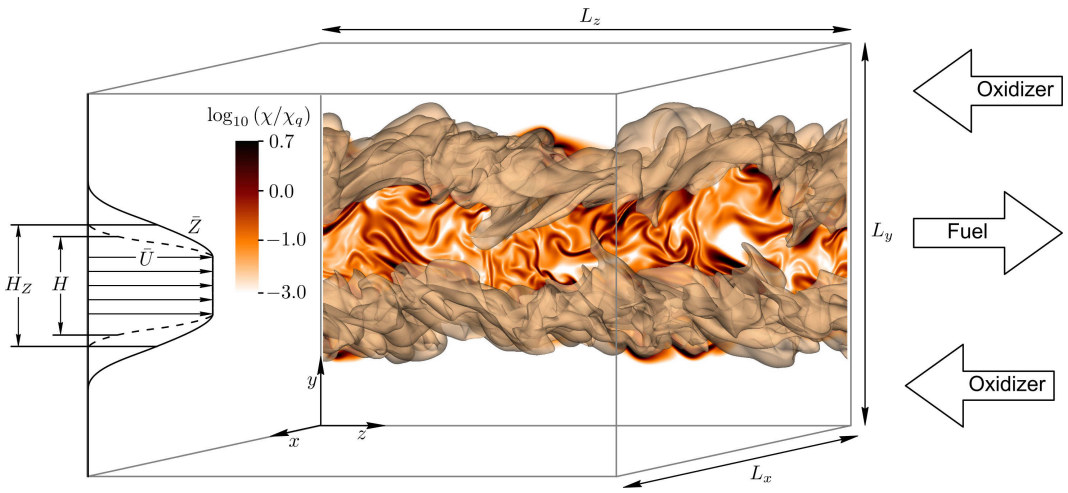

FIG. 2. Illustration of DNS setup. The figure shows that the initial mean mixture fraction profile is wider than the initial mean stream-wise velocity profile.

II. DIRECT NUMERICAL SIMULATION OF A TURBULENT NON-PREMIXED JET FLAME

A direct numerical simulation (DNS) of a turbulent temporally-evolving planar CO/H_2 jet flame has been carried out with a setup closely related to case H of Hawkes *et al.*[7]. The flow configuration is illustrated schematically in fig. 2. The fuel stream is composed of 50% CO, 10% H_2, and 40% N_2 by volume. The oxidizer stream, surrounding the fuel stream, is composed of 25% O_2 and 75% N_2. The stoichiometric mixture fraction equals $Z_{\mathrm{st}} = 0.42$, thus being located in the shear layer of the jet in a region of high turbulence intensity. Chemical kinetics are represented by a reduced mechanism with 21 reactions and 11 species, see Li[8].

The DNS solves the transport equations for momentum, temperature, and species in a low-mach number formulation. Spatial derivatives are computed by a sixth order explicit scheme, and temporal integration is performed by an explicit fourth-order low-storage Runge-Kutta scheme. The Poisson equation for the pressure is solved in spectral space. Details of the numerical procedure are summarized by Abdelsamie *et al.*[9] and Abdelsamie and Thevenin[10]. The DNS employs a rectangular geometry with periodic boundary conditions in stream-wise and span-wise directions, and outlet boundary conditions in cross-wise direction. The governing equations are discretized on a structured uniform mesh with $512 \times 1025 \times 1024$ grid points, in span-wise, cross-wise, and stream-wise directions, respectively. The size of the computational domain is $7H_0 \times 14H_0 \times 14H_0$, where H_0 denotes the initial jet width.

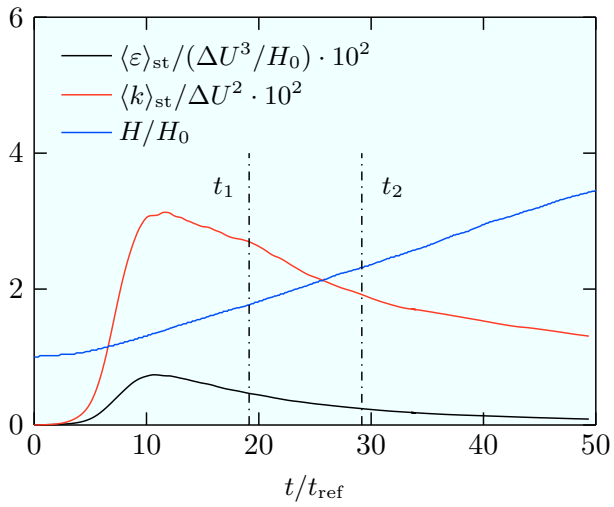

FIG. 3. Temporal evolution of jet height H, mean dissipation $\langle\varepsilon\rangle_{\rm st}$, and mean turbulent kinetic energy $\langle k\rangle_{\rm st}$. The ensemble-averages are conditioned on a small band, $0.8Z_{\rm st} < Z < 1.2Z_{\rm st}$, around stoichiometric mixture and normalized with the initial velocity difference ΔU_0 and the initial jet width H_0. Note that $\langle\varepsilon\rangle_{\rm st}$ and $\langle k\rangle_{\rm st}$ are scaled by a factor of 100. The time steps considered for analysis are indicated by the vertical dashed lines.

The jet width H is defined as the distance between the points, where the mean cross-stream velocity profile declines to 50% of the center-line value. Similar to the reference case[7] we triggered turbulence by initializing a broadband random Gaussian velocity field that is filtered outside the jet core. The initial cold-flow Reynolds number, based on the initial jet width H_0, the initial velocity difference $\Delta U_0 = U_{\rm fuel} - U_{\rm oxidizer}$, and the pure fuel viscosity ν_f is close to $\mathrm{Re}_0 = 9075$. Resolving the smallest scales of turbulent flows by the numerical grid is crucial for the accuracy of the DNS and the subsequent analysis by the method of dissipation elements. For the time steps t_1 and t_2 indicated in fig. 3 the ratio $\eta/\Delta x$ at the center plane of the jet equals 0.93 and 1.39, respectively, where η denotes the Kolmogorov length scale, and Δx denotes the uniform grid width.

Let us now briefly analyze the temporal evolution of the turbulent jet flow. To account for the interaction between chemistry and turbulence we introduce an ensemble-average conditioned on a small band, $0.8Z_{\rm st} < Z < 1.2Z_{\rm st}$, centered around stoichiometric mixture (denoted by $\langle\cdot\rangle_{\rm st}$). The temporal evolution of the mean turbulent energy $\langle k\rangle_{\rm st}$ and the mean dissipation $\langle\varepsilon\rangle_{\rm st}$ are shown in fig. 3. Both curves are normalized by the initial values ΔU_0 and H_0 and exhibit an initial transient before turbulence turns into a decaying state beginning

with $t/t_{\mathrm{ref}} \approx 10$. The reference time scale is defined as

$$t_{\mathrm{ref}} = \frac{H_0}{\Delta U_0}\,. \tag{11}$$

Additionally, fig. 3 shows the non-dimensional jet width H/H_0, where after an initial transient a linear growth is observed.

In the following we present an analysis based on two different time steps at $t_1 = 19\,t_{\mathrm{ref}}$ and $t_2 = 29\,t_{\mathrm{ref}}$. At these time steps chemistry interacts with fully developed decaying turbulence.

III. ZONAL DECOMPOSITION

The aim of the present section is to perform a physically motivated zonal decomposition of the turbulent jet flow based on the ending points of dissipation elements.

We adapted the algorithm developed by Wang and Peters[5] to trace gradient trajectories on the instantaneous mixture fraction field of the turbulent jet flow. The present analysis required modifications of the algorithm as the original work studied homogeneous shear turbulence in a triply periodic box. The jet flow under consideration is inhomogeneous in cross-stream direction and reveals a complex morphology with a fully developed turbulent core region adjacent to an outer irrotational region. Some gradient trajectories originating from the turbulent core enter the irrotational region and may proceed further without reaching an extremal point. The tracing of these trajectories is therefore stopped when a mixture fraction threshold $Z \leq 0.05$ is attained.

Mellado, Wang, and Peters[11] applied gradient trajectory analysis to perform a spatial partitioning of a temporally-evolving turbulent shear flow in an outer irrotational regime and an inner fully developed turbulent regime. The transition between the turbulent and non-turbulent region occurs across a thin layer of finite size, which was referred to as the turbulent/non-turbulent interface (T/NT)[12,13]. In a turbulent non-premixed flame a second interface of finite thickness, namely the reaction zone, can be identified in the vicinity of stoichiometric mixture, dividing the mixture fraction field into a fuel lean and a fuel rich zone. The reaction zone becomes singular in the limit of infinitely fast chemistry. For finite rate chemistry the local thickness of the reaction zone depends on the Damköhler number. A strong interaction with turbulence or slow chemistry results in a broadening of the reaction zone.

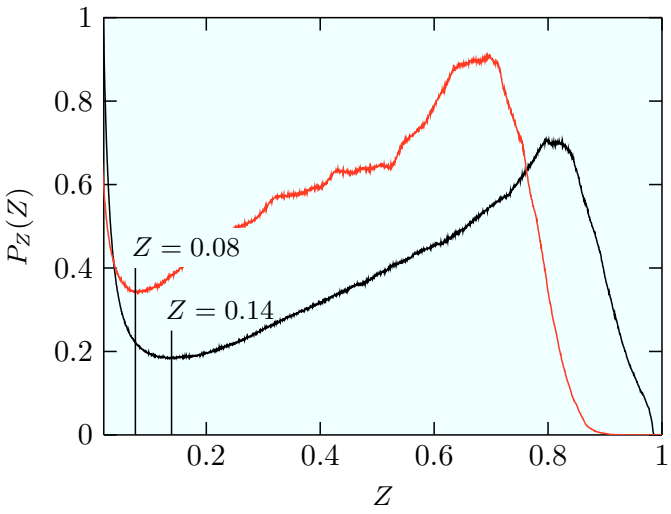

FIG. 4. Marginal probability distribution of the mixture fraction $P(Z)$ at t_1 (black) and t_2 (red). Both pdf exhibit a bimodal shape with a minimum located at $Z = 0.14$ and $Z = 0.08$, respectively.

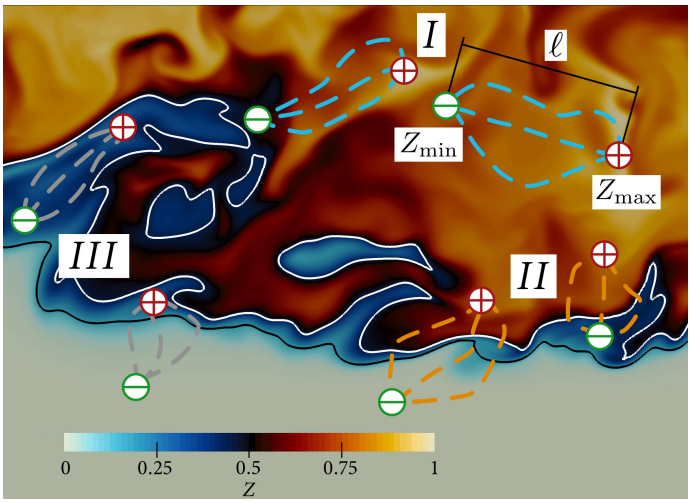

FIG. 5. Two-dimensional slice of the instantaneous mixture fraction field Z in the y-z plane at $t/t_{\text{ref}} = 19$. Gradient trajectories are schematically shown in the different regimes by colored dashed lines. The white line indicates the location of stoichiometric mixture fraction and the black line indicates the location of the T/NT-interface. Note that gradient trajectories from regime II and III can cross the T/NT-interface and enter the irrotational outer region.

We partition the turbulent jet flame into three different regimes (numbered by I, II and III) based on the value of the mixture fraction at the ending points of the trajectories. It is important to note that all gradient trajectories from a dissipation element belong to

the same regime as the zonal decomposition is based solely on the ending points. The partitioning allows us to discriminate between dissipation elements that are subject to chemical reaction and those that are mainly subject to turbulent mixing. The decomposition based on dissipation elements is self-contained and has the properties of completeness and uniqueness. This means that each material point should be included once and only once in the decomposed object[14,15].

The first regime (I) is defined as the inner, fuel rich core region of the jet, where gradient trajectories do not cross the iso-surface of stoichiometric mixture, i.e. $1 \geq Z_{\mathrm{max}} > Z_{\mathrm{min}} > Z_{\mathrm{st}}$. In this regime turbulent mixing prevails compared to chemical reaction. For the present study, the value of Z_{st} is about 0.42 yielding the iso-surface of stoichiometric mixture being located in the fully developed turbulent part of the jet flow. The second regime (II) contains all dissipation elements that cross the iso-surface of stoichiometric mixture. Trajectories in this regime are subject to both turbulent mixing and chemical reaction. These dissipation elements connect a maximum point at the fuel rich side with $Z_{\mathrm{max}} > Z_{\mathrm{st}}$ and a minimum point at the fuel lean side with $Z_{\mathrm{min}} < Z_{\mathrm{st}}$. Trajectories intersecting the iso-surface of stoichiometric mixture provide information about the flame structure not only in the vicinity of the stoichiometric surface, but also further away from it. In other words: the two-point character of gradient trajectories provides information whether a point away from stoichiometric mixture is connected through a diffusive layer with the reaction zone. This feature is important for the following statistical analysis. Beyond the surface of stoichiometric mixture, there is a third regime (III) for dissipation elements with $0 \leq Z_{\mathrm{min}} < Z_{\mathrm{max}} < Z_{\mathrm{st}}$. This regime lies in the fuel lean region of the jet where turbulent mixing prevails over chemical reaction. Additionally, the edge of the turbulent jet flow is characterized by a second interface dividing the flow in a non-turbulent outer region and a fully developed turbulent inner region. The location of the T/NT-interface has been determined by following the procedure described by Prasad and Sreenivasan[16], who defined the location of the T/NT-interface in mixture fraction space as the local minimum of the bimodal shaped marginal mixture fraction probability density function (pdf) $P(Z)$. This pdf is displayed in fig. 4 and shows that the minimum is located at $Z = 0.14$ for t_1 and at $Z = 0.08$ for t_2. Trajectories originating from regime (II) and (III) can cross the T/NT-interface and enter the irrotational outer region. On the other hand, that means only trajectories that do not cross the T/NT-interface experience turbulent mixing over their whole length. Figure 5 illustrates the zonal decomposition by

means of a two-dimensional representation of the mixture fraction field in the y-z plane. Dissipation elements in the different regimes are illustrated schematically by bold colored lines. For notational convenience the ensemble of all dissipation elements belonging to regimes I-III is denoted as regime IV.

Let us now analyze the different regimes in mixture fraction space by the statistics of Z_m and ΔZ. The jpdf $P(Z_\mathrm{m}, \Delta Z)$ illustrates the effect of turbulent mixing and provides information where dissipation elements are precisely located in mixture fraction space. Figure 6 shows $P(Z_\mathrm{m}, \Delta Z)$ for both time steps t_1 and t_2. The jpdf reveals a triangular shape with sharp boundaries, where the boundaries are imposed through the boundedness of the mixture fraction. They obey the conditions $Z_\mathrm{m} = \Delta Z/2$ and $Z_\mathrm{m} = -\Delta Z/2 + Z_\mathrm{max}$, with Z_max being the maximum value of the mixture fraction field. During the temporal decay of the jet, Z_max decreases from $Z_\mathrm{max} = 0.99$ for t_1 to $Z_\mathrm{max} = 0.94$ for t_2. The intersection between the regime boundary lines imposes an upper limit for ΔZ, which moves to lower values during decay of the jet flow. As a consequence, the jpdf becomes singular at $\Delta Z = 0$ in the limit $t \to \infty$. Figure 6 also displays the regime borders. The boundary between regimes I and II (black dashed-dotted line) obeys the relation $Z_\mathrm{m} = \Delta Z/2 + Z_\mathrm{st}$, while the boundary between regimes II and III (black dashed line) is determined by $Z_\mathrm{m} = -\Delta Z/2 + Z_\mathrm{st}$. As the regime boundaries depend solely on Z_st they do not change with time. By definition, gradient trajectories from regime I and from regime III cannot intersect the surface of stoichiometric mixture.

For the first time step t_1, the jpdf $P(Z_\mathrm{m}, \Delta Z)$ exhibits a distinct maximum around $\Delta Z = 0.2$ and $Z_\mathrm{m} = 0.85$ indicating that most dissipation elements have a relatively small scalar difference and are situated in a fuel rich region in regime I. On the other hand, there are also dissipation elements spanning a scalar difference close to unity. Owing to the regime decomposition these dissipation elements belong to regime II. During the turbulent mixing process this distinct maximum disappears and new dissipation elements are generated with different pairs of Z_m and ΔZ, cf. fig. 6(right).

IV. STATISTICAL ANALYSIS OF DISSIPATION ELEMENTS

In the following we employ the zonal decomposition and discuss statistical properties of dissipation elements in different regimes of the jet. Table I summarizes global statistical

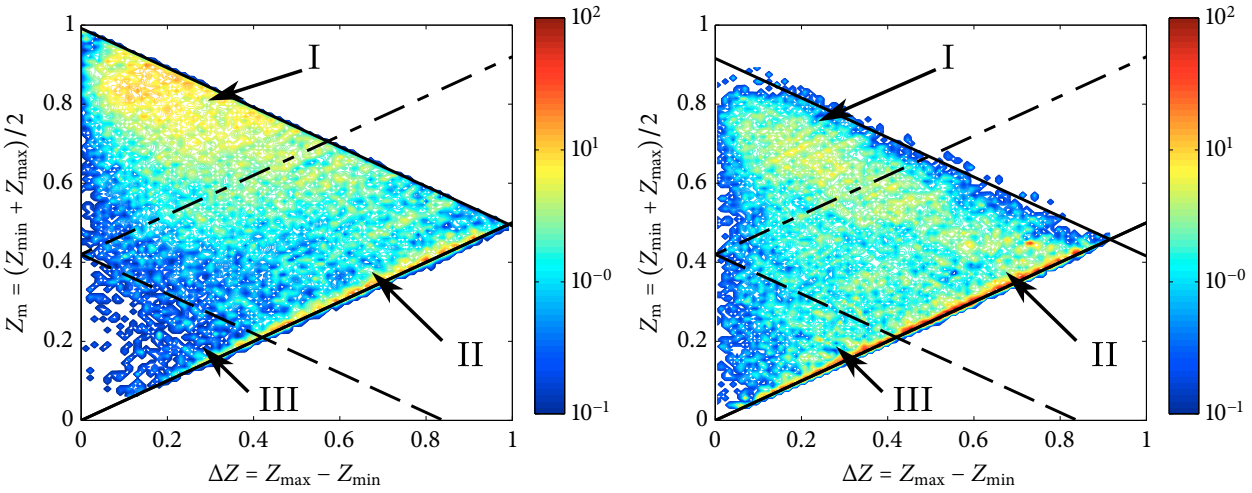

FIG. 6. Joint pdf of Z_m and ΔZ for t_1 (left) and t_2 (right). The jpdfs reveal a triangular shape with sharp borders imposed by the boundedness of the mixture fraction (black solid lines). Also the different regimes and the regime boundaries (dashed lines) are indicated.

properties of dissipation elements obtained from the different regimes for both time steps under consideration. For both time steps, the largest mean length ℓ_m is observed for trajectories from regime II, since only these trajectories can connect the turbulent core region with the irrotational outer flow. The normalized mean length $\ell_m^* = \ell_m/H_0$ increases for all regimes with time which comes from an increase of turbulent length scales during the decay process of the jet flow. Additionally, tab. I indicates the normalized mean mixture fraction difference $\langle \Delta Z^* \rangle = \langle \Delta Z \rangle / \Delta Z_0$, the normalized mean mixture fraction between the extremal points $\langle Z_\mathrm{m}^* \rangle = \langle Z_\mathrm{m} \rangle / \Delta Z_0$, and the normalized mean gradient $\langle g^* \rangle$ defined as

$$\langle g^* \rangle = \frac{\langle g \rangle}{\frac{\Delta Z_0}{H_0}} \,. \tag{12}$$

Angular brackets denote a dissipation element based ensemble-average. In the following, all quantities marked with an asterisk are normalized by the initial jet width H_0, the initial velocity difference ΔU_0, and the initial mixture fraction difference ΔZ_0. It is notable that regime II has the highest mean scalar difference $\langle \Delta Z^* \rangle$ and the highest mean gradient $\langle g^* \rangle$.

A. Joint Distributions of ΔZ and ℓ

Additional information about the local structure of the turbulent mixture field is provided by the joint statistics of the length ℓ and the scalar difference ΔZ. These two quantities are

TABLE I. Parameters of dissipation elements for time step t_1 (left) and t_2 (right), listed for the fuel rich regime (I), the stoichiometric regime (II), and the fuel lean regime (III). The ensemble of all regimes is denoted by "all".

	I	II	III	all
ℓ_m/H_0	0.39	0.49	0.16	0.41
$\langle \Delta Z^* \rangle$	0.23	0.58	0.09	0.35
$\langle Z^*_\mathrm{m} \rangle$	0.76	0.46	0.06	0.58
$\langle g^* \rangle$	0.70	1.64	0.44	1.05

	I	II	III	all
ℓ_m/H_0	0.54	0.60	0.22	0.45
$\langle \Delta Z^* \rangle$	0.20	0.53	0.10	0.32
$\langle Z^*_\mathrm{m} \rangle$	0.67	0.38	0.07	0.31
$\langle g^* \rangle$	0.44	1.19	0.31	0.75

the object of interest here. The normalized jpdf $P(\Delta Z^*, \ell^*)$ and the normalized conditional average $\langle \Delta Z^* | \ell^* \rangle$ are shown in fig. 7 for all regimes. It is seen that ΔZ^* and ℓ^* are not independent and that long dissipation elements have on average also a large scalar difference ΔZ^*. This finding is also supported by the conditional mean $\langle \Delta Z^* | \ell^* \rangle$, which increases monotonously with ℓ^*. The jpdf $P(\Delta Z^*, \ell^*)$ illustrates different physical effects. The upper left corner of the jpdf, where ℓ^* is small but ΔZ^* attains already large values close to unity, represents poorly mixed regions, where the mean gradients $g = \Delta Z/\ell$ are large. Well mixed regions occur at the lower left edge of the jpdf where ΔZ^* becomes small at a finite length scale ℓ^*. This region is pronounced for regimes I and III but is less significant for regime II. The jpdf $P(\Delta Z^*, \ell^*)$ exhibits a maximum, which is located around $\ell^* \approx 0.3$ and $\Delta Z^* \approx 0.2$ for regimes I and III, and at the same length scale but at a significantly higher value of $\Delta Z^* \approx 0.5$ for regime II. Hence, dissipation elements from regime II connect especially extremal points with a higher scalar difference. This finding is supported by the considerably larger mean mixture fraction difference $\langle \Delta Z^* \rangle$ for regime II given in tab. I. From this finding the question arises in which regime and at which length scale large mean gradients g will occur.

B. Joint Distributions of g and ℓ

From dimensional arguments, the mean gradient g and the scalar dissipation χ are related, cf. eq. (10). Therefore, the jpdf $P(g, \ell)$ is of interest and provides a scale-dependent information about the mixing rate of turbulent flows. The jpdfs of the normalized mean

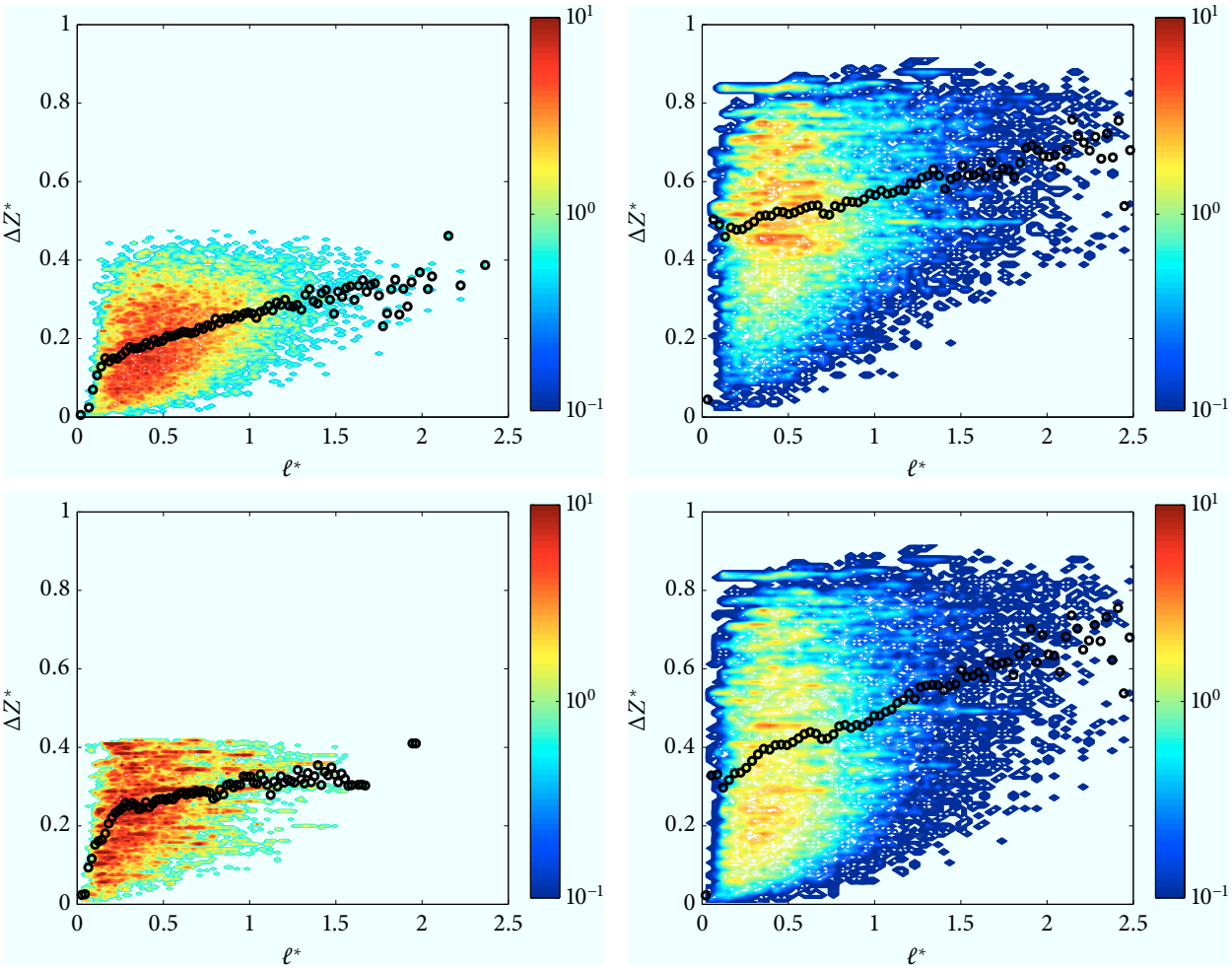

FIG. 7. Normalized joint pdf of ΔZ^* and ℓ^* for regimes I, II (top,left to right), and regime III and the ensemble of all dissipation elements (bottom, left to right) for t_2. The conditional mean $\langle \Delta Z^* | \ell^* \rangle$ is indicated by black circles.

gradient g^* and the normalized length ℓ^* are shown in fig. 8 for all regimes. The contour levels are scaled logarithmically. With respect to g^* the jpdfs exhibit a long tail meaning that very large but rare excursions from the mean value $\langle g^* \rangle$ occur. In the literature this phenomenon is known as internal intermittency, see Sreenivasan and Antonia [17] and Warhaft [18]. The tail of $P(g^*, \ell^*)$ is most pronounced for regime II, where large mean gradients g^* (which are as large as 8 times the reference value $\Delta Z_0 / H_0$) are situated at an intermediate length scale and not in the limit $\ell^* \to 0$. This results from the fact that ΔZ^* and ℓ^* are not independent, and that ΔZ^* is affected by molecular damping at the smallest scales. Despite averaged over the length of a dissipation element, the mean gradient g^* is a highly intermittent quantity. Relatively steep jumps in the mixture fraction value manifest themselves as cliff-like structures. They

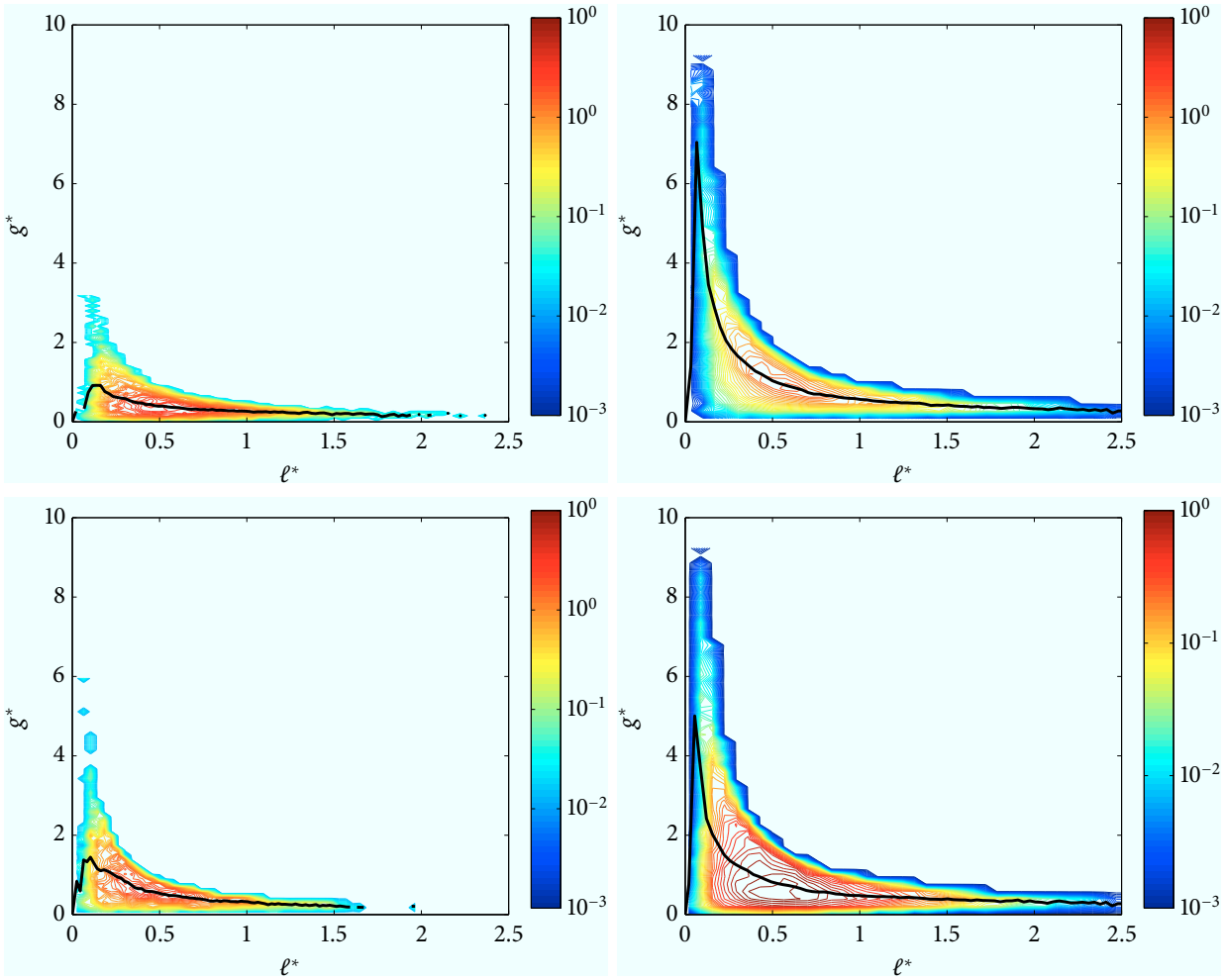

FIG. 8. Normalized joint pdf of g^* and ℓ^* for regimes I, II (top, left to right), regime III and the ensemble of all dissipation elements (bottom, left to right) with logarithmically scaled color-level for t_2. The conditional mean $\langle g^*|\ell^*\rangle$ is indicated by a black line.

show-up primarily in thin, highly confined layers, which are typically formed by a compressive straining motion, cf. Brethouwer, Hunt, and Nieuwstadt [19] and Ishihara, Kaneda, and Hunt [20]. The width of these hardly mixed layers can be defined as the length scale ℓ^* at which the maximum value of the conditional mean $\langle g^*|\ell^*\rangle$ occurs and equals approximately $\ell^* \approx 0.1$ independently of the regime. Strong molecular transport in the direction along gradient trajectories takes place predominantly over this length scale. On the other hand, ramp-like structures are found in fig. 8 at the lower right tail of the joint pdf. There, the scalar difference ΔZ^* varies monotonously over a length scale of more than $\ell^* = 2.5$, which equals roughly the size of the jet width at the considered time step t_2, cf. fig. 3.

V. COMPRESSIVE AND EXTENSIVE STRAIN ALONG DISSIPATION ELEMENTS

The generation of cliff-like structures in the turbulent mixing field is driven by a straining motion over an intermediate length scale[19,21]. This finding results from a preferential alignment of the scalar gradient with the direction of the most compressive strain rate[22]. The relevant mechanism for a distortion of dissipation elements is a velocity difference Δu_n between the ending points, which results in a change of the length ℓ. Only a velocity difference directed along the line connecting the extremal points can cause this length change. Figure 9 shows the conditional strain rate a_ℓ normalized by its asymptotic value $a_\infty = a_\ell(\ell \to \infty)$ for all regimes as a function of ℓ^*. The curves show the characteristic shape already found for dissipation elements in non-reactive flows, see Gampert *et al.*[23] and Wang[24]. The conditional strain rate is negative for small elements with $\ell^* < 0.2$ indicating that small elements are on average subject to compressive strain. For longer elements with $\ell^* > 0.5$, the strain rate a_ℓ becomes positive and tends to a constant value a_∞. These elements are on average subject to extensive strain. Additionally, we observe that a normalization with a_∞ allows for a very good collapse of all curves independently of the regime.

To explain the formation of gradients in dissipation elements in more detail a balance between gradient production and gradient dissipation is examined. The temporal macroscopic change of g for an individual dissipation element can be written as

$$\frac{\mathrm{d}g}{\mathrm{d}t} = \frac{1}{\ell}\frac{\mathrm{d}\Delta Z}{\mathrm{d}t} - \frac{\Delta Z}{\ell^2}\frac{\mathrm{d}\ell}{\mathrm{d}t}\,. \tag{13}$$

A change of ΔZ is attributed to diffusion and predominantly takes place at small scales where the gradient between the extremal points is very steep. An analytical expression for this term was derived by Wang[15] by analyzing the relative motion of two adjacent extremal points in the limit of small scales. In three dimensions it reads

$$\frac{\mathrm{d}\Delta Z}{\mathrm{d}t} = -12D\frac{\Delta Z}{\ell^2}\,. \tag{14}$$

The negative sign indicates that diffusivity results in a reduction of the scalar difference ΔZ between adjacent extremal points and thus to a destruction of g. At larger scales the relevant mechanism for a temporal change of g stems from a velocity difference Δu_n between the ending points of a dissipation element. A compressive strain acting on dissipation elements

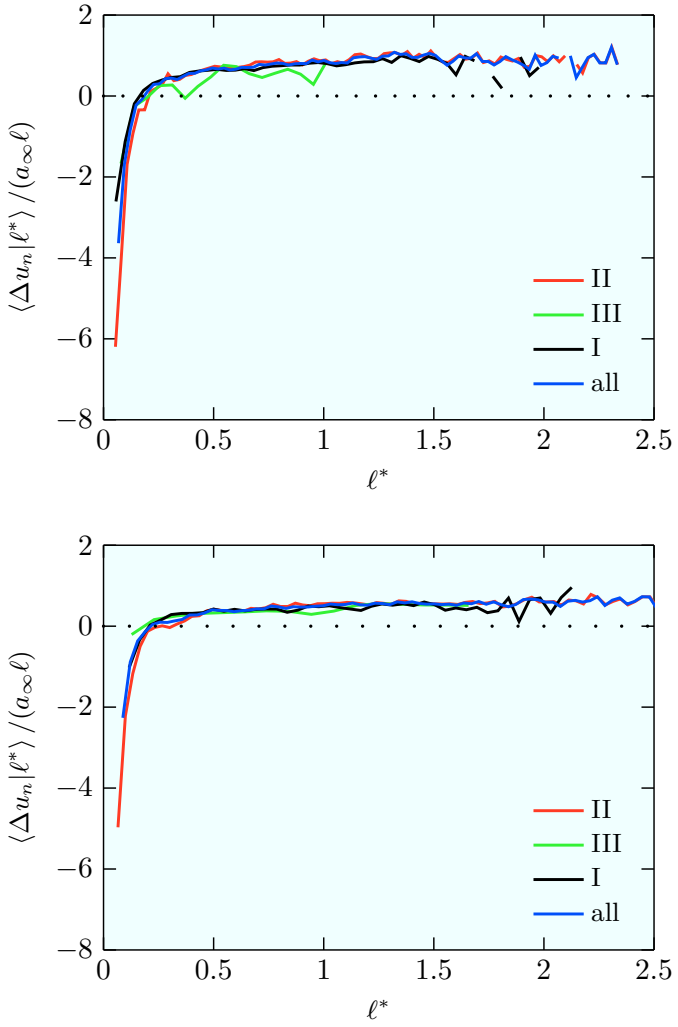

FIG. 9. Normalized conditional strain rate $a_\ell/a_\infty = \langle \Delta u_n | \ell^* \rangle / (a_\infty \ell)$, for all regimes for t_1 (top) and t_2 (bottom).

shortens the distance ℓ between maximum and minimum point. During this process the scalar difference ΔZ remains virtually unchanged, so that compressive strain leads to an increase of g. Hence, the temporal change of ℓ in eq. (13) can be written as

$$\frac{\mathrm{d}\ell}{\mathrm{d}t} = \Delta u_n \,. \tag{15}$$

In agreement with Kolmogorov's second hypothesis[25,26] the turbulent motion at larger scales is independent of the molecular diffusivity D. Using eqs. (15) and (14) in eq. (13) gives

$$\frac{\mathrm{d}g}{\mathrm{d}t} = -12D\frac{g}{\ell^2} - a_\ell g \,, \tag{16}$$

where the first term on the right hand side can be interpreted as a destruction of g due to diffusivity and the second term as a production of g due to strain.

To further examine the destruction and production of g, eq. (16) is conditioned on the length-scale ℓ and written normalized by H_0, ΔU_0 and ΔZ_0, i.e.

$$\frac{\mathrm{d}\langle g^*|\ell^*\rangle}{\mathrm{d}t^*} = \underbrace{-12Pe^{-1}\langle\frac{g^*}{\ell^{*2}}|\ell^*\rangle}_{\mathcal{D}^*_\ell} \underbrace{-\langle a^*_\ell g^*|\ell^*\rangle}_{\mathcal{P}^*_\ell}, \tag{17}$$

where the Peclet number is defined as

$$Pe = \frac{\Delta U_0 H_0}{D}. \tag{18}$$

The gradient $\langle g^*|\ell^*\rangle$, and its production $\mathcal{P}^*_\ell$ and destruction $\mathcal{D}^*_\ell$ are shown as a function of ℓ^* in fig. 10. It is seen that $\mathcal{D}^*_\ell$ increases monotonously towards smaller scales. This underlines the small-scale nature of $\mathcal{D}^*_\ell$, which becomes effective when the gradient steepens. On the other hand, $\mathcal{P}^*_\ell$ reveals a distinct maximum at a finite length scale $\ell^* = 0.1$ and drops to zero towards the origin. The peaks of $\langle g^*|\ell^*\rangle$ and $\mathcal{P}^*_\ell$ occur at the same length scale indicating that $\mathcal{P}^*_\ell$ induces the formation of g^*. Moreover, $\mathcal{P}^*_\ell$ becomes negative at larger scales and turns into a moderate sink term, since larger scales are dominated on average by extensive strain, cf. fig. 9. The effect of fast processes (cf. Schaefer *et al.*[27]) is not covered by eq. (17). By splitting or reconnection processes new dissipation elements with different mean gradients are generated at new length scales, cf. fig. 11. This explains why the mean gradient $\langle g^*|\ell^*\rangle$ declines slowly towards larger scales while the gradient production $\mathcal{P}^*_\ell$ due to slow processes acts mainly localized at smaller length scales.

Combining these findings allows us to refine the understanding of the formation of the mean gradient $\langle g^*|\ell^*\rangle$ of dissipation elements. In agreement with the enhanced gradient production towards small scales, $\langle g^*|\ell^*\rangle$ reveals a steady increase towards smaller scales until the damping effect of diffusivity cuts in at the smallest scales. The balance between production through compressive strain and destruction of g^* through molecular damping results in the characteristic shape of $\langle g^*|\ell^*\rangle$ with a steep decline towards the origin and a distinct maximum at a finite length scale. It is noteworthy that the gradient based on the scalar increment

$$\frac{\delta_r Z}{r} = \frac{Z(\boldsymbol{x}+\boldsymbol{r}) - Z(\boldsymbol{x})}{r} \tag{19}$$

reveals a different limiting behavior for $r \to 0$, as for arbitrary even moments the limit

$$\lim_{r\to 0} \frac{\langle(\delta_r Z)^{2n}\rangle}{r^{2n}} = \langle\left(\frac{\partial Z}{\partial x}\right)^{2n}\rangle \tag{20}$$

tends to the respective non-zero scalar gradient moment.

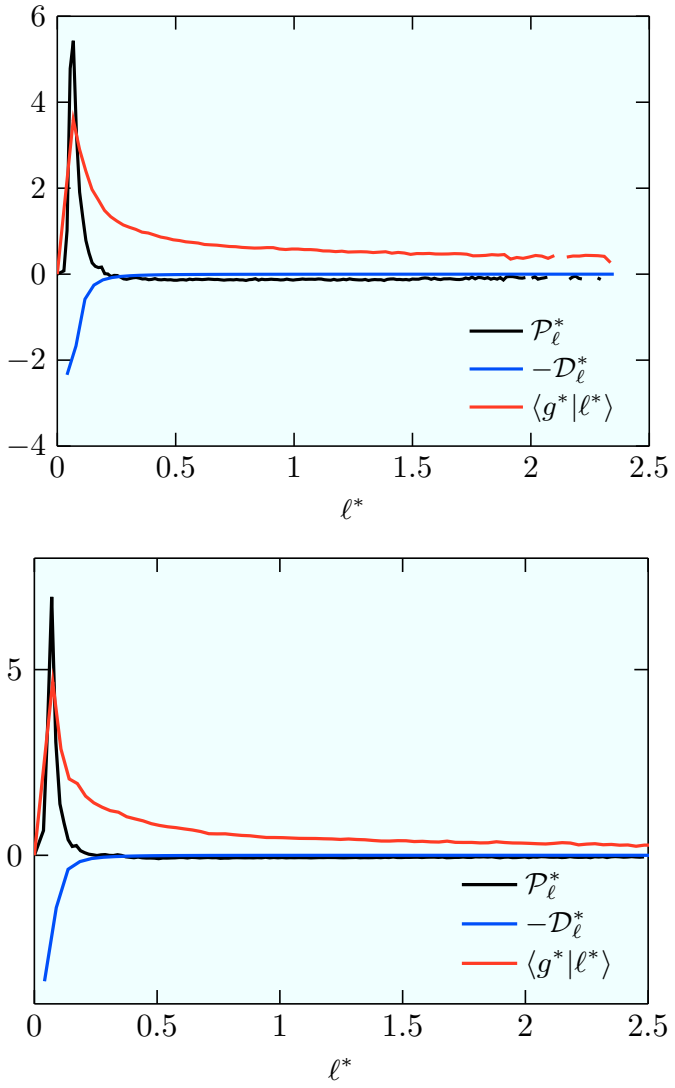

FIG. 10. Balance between the normalized conditional gradient production $\mathcal{P}^*_\ell$ and gradient dissipation $\mathcal{D}^*_\ell$ for time step t_1 (top) and t_2 (bottom). Additionally the normalized conditional mean gradient $\langle g^*|\ell^*\rangle$ is shown.

VI. THE INNER STRUCTURE OF DISSIPATION ELEMENTS

Chemical reaction takes place in thin confined layers around stoichiometric mixture. In order to accurately describe chemical reactions additional information about the inner structure of dissipation elements is necessary. This information is provided by analyzing individual gradient trajectories. The zonal decomposition, cf. sec. III, provides additional information, whether gradient trajectories are connected with the stoichiometric surface.

Let us now apply zonal statistics of gradient trajectories to show how chemical reactions

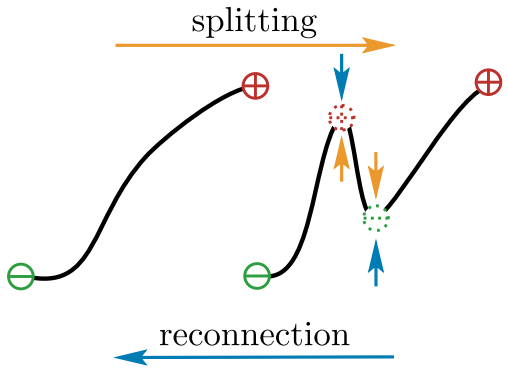

FIG. 11. Illustration of a splitting and a reconection event in one-dimensional space. By splitting one large dissipation element is cut in three small elements. By reconnection smaller dissipation elements are joint together and one large element appears.

are affected by turbulence. To do so, we trace all gradient trajectories and restrict the analysis to gradient trajectories belonging to regime II, since only these gradient trajectories intersect the stoichiometric surface and have the ability to burn.

Figure 12 shows the dependence of the mean maximum temperature $\langle T_{\max}\rangle/T_q$ computed over all trajectories of regime II on the mean gradient g^* for the two time steps under consideration. It is clearly seen for both time steps that an increase of g^* leads to a decrease of $\langle T_{\max}\rangle/T_q$. For large values of g^* the diffusive transport along the trajectory is enhanced, which reduces $\langle T_{\max}\rangle/T_q$ and results in quenching when $\langle T_{\max}\rangle/T_q$ falls below unity. This phenomenon is well known in the context of flamelet models, where the conditional scalar dissipation $\langle\chi|Z\rangle$ acts as a diffusivity in mixture fraction space and affects the temperature[28]. The temperature declines with increasing scalar dissipation rate until a critical value of the scalar dissipation rate χ_q is attained. Extinction occurs for values above χ_q. The analogy between the flamelet parameter $\langle\chi|Z\rangle$ and g^* underlines the relevance of dissipation elements for the parameterization of non-premixed turbulent flames. For the later time step the shape of $\langle T_{\max}\rangle/T_q$ is very similar to the early time step but situated at a higher temperature level. This is due to the fact that the global scalar dissipation is decreasing at later times causing a re-ignition of the flame.

Further details about the impact of local fluctuations of the mixture fraction field on chemistry can be obtained by examining statistics of chemical species. Here, we consider the mass fraction of the species OH, which is often utilized as a marker for the flame position. Figure 13 shows the joint pdf of the mass fraction Y_{OH} and the normalized gradient g^*

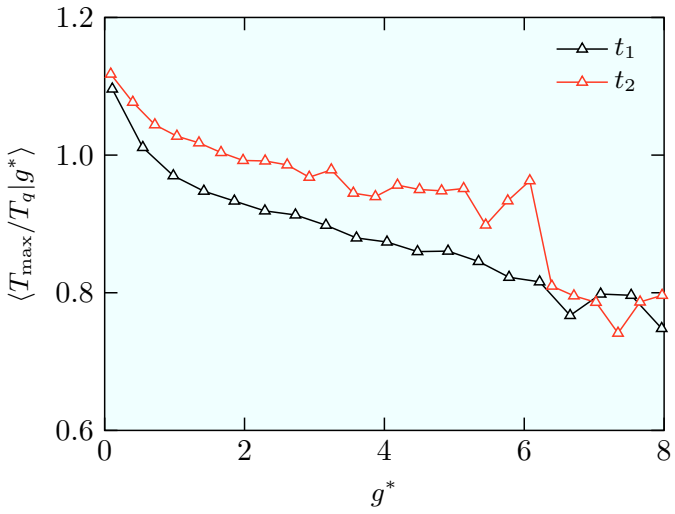

FIG. 12. Maximum temperature $\langle T_{\max}/T_q|g^*\rangle$ of trajectories belonging to regime II as a function of the normalized gradient g^* for the two different time steps t_1 and t_2. The temperature is normalized by the quenching temperature $T_q = 1303\,\mathrm{K}$.

conditioned on trajectories belonging to regime II. The OH mass fraction is normalized by its quenching value $Y_{\mathrm{OH,q}}$, which is obtained from a one-dimensional flamelet calculation under conditions similar to the DNS. Trajectories with $Y_{\mathrm{OH}}/Y_{\mathrm{OH,q}} < 1$ are considered to be quenched. The joint pdf reveals for both time steps strong fluctuations around the conditional mean value $\langle Y_{\mathrm{OH}}/Y_{\mathrm{OH,q}}|g^*\rangle$. Especially for smaller values of g^*, i.e. $g^* < 6$, both burning and quenched states can be observed. For $g^* > 6$, nearly all trajectories are quenched, which is in agreement with the behavior of $\langle T_{\max}|g^*\rangle$ discussed before. These findings signify that not only the local mixing state determines chemistry, but also the time history, at which the mixing state is reached. Similar conlcusions were drawn by Scholtissek *et al.*[29] by analyzing the temporal evolution of individual gradient trajectories in a turbulent non-premixed jet flame.

In a next step, the inner structure of gradient trajectories is studied by the conditional average of the scalar dissipation $\langle\chi|Z\rangle$. The conditional scalar dissipation is of interest in the context of flamelet models, where it has to be specified as an external parameter. By knowing the precise path of gradient trajectories, we can restrict our analysis to trajectories from regime II and further discriminate between burning and non-burning trajectories. Burning trajectories are defined as those trajectories whose local maximum temperature $T_{\max}$ exceeds the quenching temperature T_q. A dissipation element can contain both "burning" and

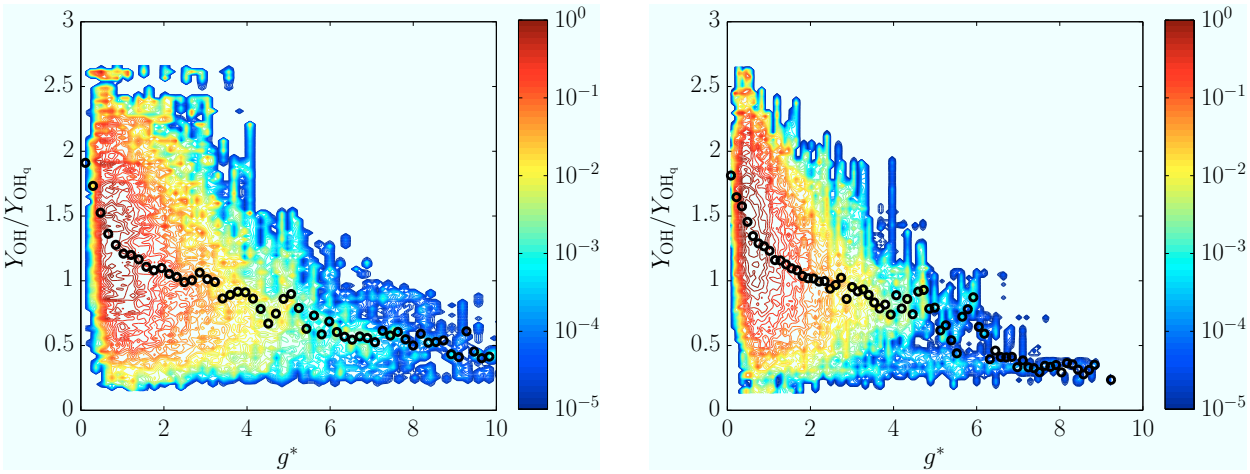

FIG. 13. Joint pdf of the mass fraction of OH and the normalized gradient g^* for different time steps t_1 (left) and t_2 (right) conditioned on trajectories belonging to regime II.

"quenched" trajectories. Figure 14 shows the conditional scalar dissipation $\langle\chi|Z\rangle$ calculated along gradient trajectories, where a distinction into burning and non-burning trajectories is displayed. It is clearly seen that "quenched trajectories" experience a significantly higher conditional scalar dissipation rate compared to "burning trajectories". Additionally, the "quenched trajectories" exhibit a bell-like shape with a maximum located close to stoichiometric mixture, while the "burning trajectories" reveal a two-hump shape. A bell-like shape is in agreement with the error-function-model, which is an analytical solution for $\langle\chi|Z\rangle$ in a counter-flow configuration[28]. A two-hump shape for $\langle\chi|Z\rangle$ was observed before by Mellado, Wang, and Peters[11] and Pantano, Sarkar, and Williams[30] in turbulent shear flows. In turbulent flames, the heat release and the associated increase of viscosity results in a damping of gradients around stoichiometric mixture favoring a two-hump shape of $\langle\chi|Z\rangle$. For "quenched trajectories" the heat release around stoichiometric mixture is lacking and the bell-like shape is preserved. This observation is relevant for flamelet models. Employing the same model for $\langle\chi|Z\rangle$ in both burning and quenched regimes may not be sufficient to correctly represent the interaction between turbulent mixing on chemistry.

VII. CONCLUDING REMARKS

Dissipation element analysis has been applied to a direct numerical simulation of a non-premixed temporally evolving jet flame. First, dissipation elements have been computed on

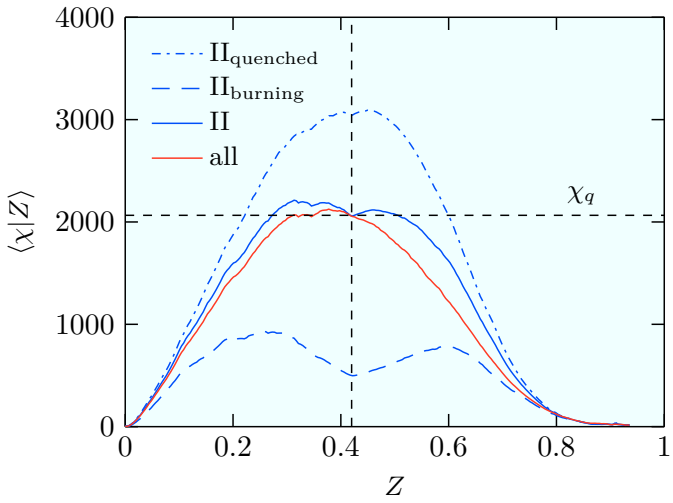

FIG. 14. Conditional average of the scalar dissipation rate $\langle\chi|Z\rangle$ for time step t_2. Additionally, for regime II, $\langle\chi|Z\rangle$ is shown for quenched and burning gradient trajectories. The vertical dashed line indicates Z_{st} and the horizontal dashed line indicates χ_q.

the mixture fraction field Z and parameterized by the arithmetic mean Z_{m} and the difference ΔZ between the ending points. Based on this parameterization a novel decomposition for turbulent reactive jet flows based on the location of the stoichiometric surface was introduced. The decomposition defines three different regimes: a fuel rich regime (denoted by regime I), a fuel lean regime (regime III), and a stoichiometric regime (regime II). The method of dissipation elements is self-contained, meaning each grid point is included once and only once in the decomposition. Due to the two-point character of dissipation elements, the decomposition contains connectivity information and allows to discern whether points away from stoichiometric mixture are connected through a diffusive layer with the reaction zone, or whether dissipation elements leave the turbulent core of the jet and enter the irrotational outer flow. Statistics of Z_{m} and ΔZ contain information about the exact location of dissipation elements in mixture fraction space. Distinct characteristics about the temporal mixing process have been illustrated by a joint pdf of Z_{m} and ΔZ. Constraints for the regime boundaries have been derived from analytic kinematic relations. It was shown that initially most dissipation elements lie in the turbulent fuel rich regime and are distributed to the other regimes during the decay of the jet.

In a next step, a regime based statistical analysis of dissipation elements was carried out. Joint statistics of length ℓ and scalar difference ΔZ between the ending points were

analyzed for the different regimes. Both quantities are correlated and is was shown that long dissipation elements have on average a large difference ΔZ. A dissipation element based gradient $g = \Delta Z/\ell$ was introduced in order to study turbulent mixing. The statistical analysis revealed that the largest gradients occur at an intermediate length scale.

Dissipation elements interact with the turbulent motion of the velocity field. To investigate the formation of the dissipation element based gradient, the velocity difference Δu_n between the ending points of dissipation elements was introduced. It was shown that small dissipation elements are subject to compressive strain while larger elements are subject to extensive strain. A kinematic equation for the mean gradient g^* has been derived to highlight the effect of diffusivity and strain on the formation of gradients in the mixture fraction field. This balance between production due to compressive strain and destruction of g^* due to molecular damping was shown to lead to the characteristic shape of $\langle g^*|\ell^*\rangle$ with a steep decline towards the origin and a distinct maximum at a finite length scale.

Through the connection to gradient trajectories, the method of dissipation elements provides a statistical characterization of flamelets, and thereby novel insight into the interaction between chemistry and turbulence. In order to describe chemical reactions the inner structure of dissipation elements has been examined by considering the path of individual gradient trajectories. By restricting the analysis to regime II it has been shown that an increasing mean gradient g reduces the maximum temperature $T_{\max}$ along gradient trajectories. Moreover, the conditional scalar dissipation $\langle \chi|Z\rangle$ has been computed for regime II, where the access to individual gradient trajectories allows to discern between burning and non-burning trajectories. The conditional scalar dissipation reveals a two-hump shape for burning gradient trajectories, and a bell-like shape at a significantly higher level for quenched gradient trajectories.

ACKNOWLEDGMENTS

The authors gratefully acknowledge computing time granted on the supercomputer JUQUEEN at Forschungszentrum Jülich[31] by the John von Neumann Institute for Computing (NIC). The authors further acknowledge the Gauss Centre for Supercomputing e.V. (www.gauss-centre.eu) for funding this project by providing computing time on the GCS Supercomputer SuperMUC at Leibniz Supercomputing Centre (LRZ, www.lrz.de) under

grant numbers: pr83xa and pr74li. Financial support is kindly acknowledged from the German Research Foundation (DFG) in the Project HA 4367/4-1.

REFERENCES

[1]N. Peters, "Laminar diffusion flamelet models in non-premixed turbulent combustion," Progress in energy and combustion science **10**, 319–339 (1984).

[2]N. Peters, "Laminar flamelet concepts in turbulent combustion," in *Symposium (International) on Combustion*, Vol. 21 (Elsevier, 1988) pp. 1231–1250.

[3]N. Peters and P. Trouillet, "On the role of quasi-one-dimensional dissipation layers in turbulent scalar mixing," Annual Research Briefs , 27–40 (2002).

[4]N. Peters, "Multiscale combustion and turbulence," Proceedings of the Combustion Institute **32**, 1–25 (2009).

[5]L. Wang and N. Peters, "The length-scale distribution function of the distance between extremal points in passive scalar turbulence," Journal of Fluid Mechanics **554**, 457–475 (2006).

[6]L. Wang and N. Peters, "Length-scale distribution functions and conditional means for various fields in turbulence," Journal of Fluid Mechanics **608**, 113–138 (2008).

[7]E. R. Hawkes, R. Sankaran, J. C. Sutherland, and J. H. Chen, "Scalar mixing in direct numerical simulations of temporally evolving plane jet flames with skeletal CO/H_2 kinetics," Proceedings of the combustion institute **31**, 1633–1640 (2007).

[8]J. Li, Ph.D. thesis, Mechanical and Aerospace Engineering Department, Princeton University (2004).

[9]A. Abdelsamie, G. Fru, T. Oster, F. Dietzsch, G. Janiga, and D. Thévenin, "Towards Direct Numerical Simulations of low-Mach number turbulent reacting and two-phase flows using Immersed Boundaries," Computers & Fluids (2016).

[10]A. Abdelsamie and D. Thevenin, "Direct numerical simulation of spray evaporation and autoignition in a temporally-evolving jet," in *Proceedings of the Combustion Institute*, Vol. 35 (Elsevier, 2016, accepted for publication).

[11]J. P. Mellado, L. Wang, and N. Peters, "Gradient trajectory analysis of a scalar field with external intermittency," Journal of Fluid Mechanics **626**, 333–365 (2009).

[12]C. B. da Silva, J. C. Hunt, I. Eames, and J. Westerweel, "Interfacial layers between regions

of different turbulence intensity," Annual Review of Fluid Mechanics **46**, 567–590 (2014).

[13]J. Westerweel, T. Hofmann, C. Fukushima, and J. Hunt, "The turbulent/non-turbulent interface at the outer boundary of a self-similar turbulent jet," Experiments in Fluids **33**, 873–878 (2002).

[14]M. Gauding, J. H. Goebbert, C. Hasse, and N. Peters, "Line segments in homogeneous scalar turbulence," Physics of Fluids **27**, 095102 (2015).

[15]L. Wang, *Geometrical description of homogeneous shear turbulence using dissipation element analysis*, Ph.D. thesis, Shaker Verlag (2008).

[16]R. Prasad and K. Sreenivasan, "Scalar interfaces in digital images of turbulent flows," Experiments in fluids **7**, 259–264 (1989).

[17]K. R. Sreenivasan and R. Antonia, "The phenomenology of small-scale turbulence," Annual review of fluid mechanics **29**, 435–472 (1997).

[18]Z. Warhaft, "Passive scalars in turbulent flows," Annual Review of Fluid Mechanics **32**, 203–240 (2000).

[19]G. Brethouwer, J. Hunt, and F. Nieuwstadt, "Micro-structure and lagrangian statistics of the scalar field with a mean gradient in isotropic turbulence," Journal of Fluid Mechanics **474**, 193–225 (2003).

[20]T. Ishihara, Y. Kaneda, and J. C. Hunt, "Thin shear layers in high Reynolds number turbulence – DNS results," Flow, turbulence and combustion **91**, 895–929 (2013).

[21]C. Tong and Z. Warhaft, "On passive scalar derivative statistics in grid turbulence," Physics of Fluids **6**, 2165–2176 (1994).

[22]W. T. Ashurst, A. Kerstein, R. Kerr, and C. Gibson, "Alignment of vorticity and scalar gradient with strain rate in simulated Navier-Stokes turbulence," Physics of Fluids (1958-1988) **30**, 2343–2353 (1987).

[23]M. Gampert, J. H. Goebbert, P. Schaefer, M. Gauding, N. Peters, F. Aldudak, and M. Oberlack, "Extensive strain along gradient trajectories in the turbulent kinetic energy field," New Journal of Physics **13**, 043012 (2011).

[24]L. Wang, "Scaling of the two-point velocity difference along scalar gradient trajectories in fluid turbulence," Physical Review E **79**, 046325 (2009).

[25]A. N. Kolmogorov, "The local structure of turbulence in incompressible viscous fluid for very large Reynolds numbers," in *Dokl. Akad. Nauk SSSR*, Vol. 30 (JSTOR, 1941) pp. 301–305.

[26]A. N. Kolmogorov, "Dissipation of energy in locally isotropic turbulence," in *Dokl. Akad. Nauk SSSR*, Vol. 32 (JSTOR, 1941) pp. 16–18.

[27]P. Schaefer, M. Gampert, L. Wang, and N. Peters, "Fast and slow changes of the length of gradient trajectories in homogeneous shear turbulence," in *Advances in Turbulence XII* (Springer, 2009) pp. 565–569.

[28]N. Peters, *Turbulent combustion* (Cambridge university press, 2000).

[29]A. Scholtissek, F. Dietzsch, M. Gauding, and C. Hasse, "In-situ tracking of mixture fraction gradient trajectories and unsteady flamelet analysis in turbulent non-premixed combustion," Combustion and Flame **175**, 243–258 (2017).

[30]C. Pantano, S. Sarkar, and F. Williams, "Mixing of a conserved scalar in a turbulent reacting shear layer," Journal of Fluid Mechanics **481**, 291–328 (2003).

[31]M. Stephan and J. Docter, "JUQUEEN: IBM Blue Gene/Q® Supercomputer System at the Jülich Supercomputing Centre," Journal of large-scale research facilities JLSRF **1**, 1 (2015).